PROCEEDINGS OF SCIENCE

High p_{T} muons from cosmic ray air showers in IceCube

The IceCube Collaboration[†],

[†] *http://icecube.wisc.edu/collaboration/authors/icrc15_icecube*

E-mail: soldin@uni-wuppertal.de

Cosmic ray air showers with primary energies above $\gtrsim 1$ TeV can produce muons with high transverse momentum ($p_{\mathrm{T}} \gtrsim 2$ GeV). These isolated muons can have large transverse separations from the shower core, up to several hundred meters. Together with the muon bundle they form a double track signature in km^3-scale neutrino telescopes such as IceCube. The muons originate from the decay of heavy hadrons, pions, and kaons produced very early in the shower development, typically in (multiple) high p_{T} jets. The separation from the core is a measure of the transverse momentum of the muon's parent particle and the muon lateral distribution depends on the composition of the incident nuclei. Hence, the composition of high energy cosmic rays can be determined from muon separation measurements. For $p_{\mathrm{T}} \gtrsim 2$ GeV particle interactions can be described in the context of perturbative quantum chromodynamics (pQCD). Thus, these muons may contribute to test pQCD predictions of high energy interactions involving intermediate nuclei.
We discuss the contributions from various hadrons produced in air showers to the high p_{T} muon flux. Based on dedicated simulations the prospects of composition measurements using high p_{T} muons in km^3-scale neutrino telescopes are studied. We present analysis methods to study laterally separated muons in IceCube with lateral separations larger than ~ 135 m.

Corresponding author: D. Soldin*,
Dept. of Physics, University of Wuppertal, 42119 Wuppertal, Germany

The 34th International Cosmic Ray Conference,
30 July - 6 August, 2015
The Hague, The Netherlands

*Speaker.

PoS(ICRC2015)256

1. Introduction

In cosmic ray air showers with energies $E_{\text{prim}} \gtrsim 1$ TeV, muons can be produced that have large transverse momentum (p_T) imparted to them by their parent particles. Depending on their energy E_μ these muons can have large angular separations $\phi \simeq p_T/E_\mu \gtrsim 0.4^\circ$ and will diverge from the shower core while traveling to the ground. After the shower has propagated to the ground, they are observable as laterally separated muons (LS muons) that arrive with the main muon bundle. The resulting lateral separation on the ground is a direct measure of the p_T of the muon's parent. The IceCube Neutrino Observatory at the geographic South Pole is a km^3-scale detector in the antarctic ice in depths of 1450 m to 2450 m [1]. LS muons with several hundred meters separation have been observed as distinct *"double track signatures"* in the detector [2], which has a minimum resolvable track separation of about 135 m. Figure 1 (left) shows a simulated LS muon event in IceCube with the typical event signature of a muon bundle accompanied by the isolated LS muon. The muon's lateral separation from the shower core is related to its p_T via

$$d_T \simeq \frac{p_T \cdot H}{E_\mu \cdot \cos(\theta)}, \tag{1.1}$$

where H is its height of production and θ the zenith angle of the arrival direction [3]. Here, and in the following, we use natural units $c = 1$. Figure 1 (right) shows the lateral separation as a function of the transverse momentum for a typical muon energy of 1 TeV at different zenith angles and interaction heights. The typical transverse momentum to produce laterally separated muons in IceCube is about 2 GeV, where parton interactions can be described in the context of perturbative quantum chromodynamics (pQCD) [2]. We consider muons with energies above $E_{\mu,\text{min}} = 460$ GeV to ensure they can reach the deep ice detector [4], and a minimum transverse momentum to produce LS muons of $p_{T,\text{min}} = 1$ GeV. In the following, the term *"high p_T"* refers to transverse momenta and energies above these thresholds.

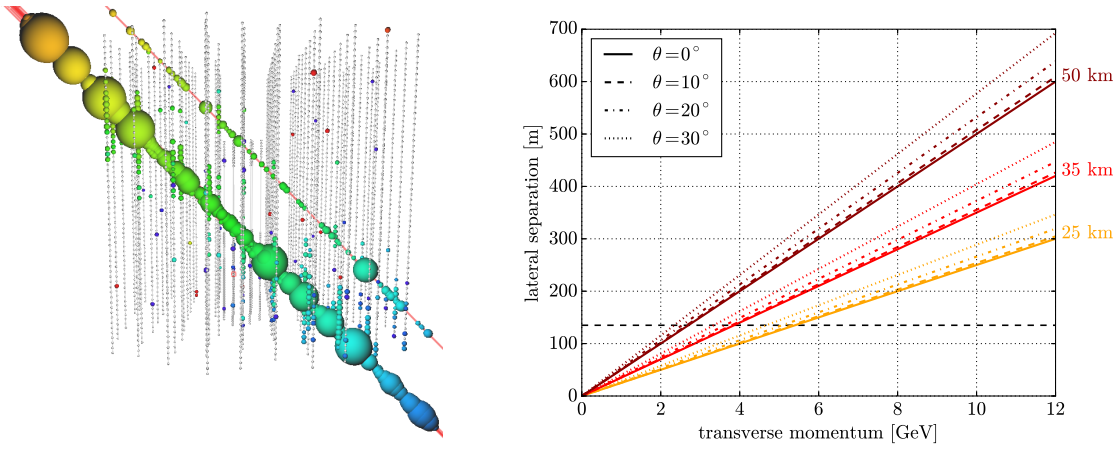

Figure 1: Left: Simulated LS muon event in the IceCube detector with a primary energy of ~ 6 PeV and $d_T = 232$ m. Small gray spheres indicate the detector DOMs and larger colored ones DOMs which triggered. Spheres along the muon tracks (red lines) show the simulated emitted light yield and colors indicate the time-ordering from red (early) to blue (late). The simulation also includes noise hits in the detector volume. Right: Lateral separation of a 1 TeV muon as a function of p_T for different zenith angles θ and interaction heights.

High p_T particles are predominantly produced in the first interaction. Hence, measurements of the lateral separation distribution of LS muons can be used to test model predictions at very high energies and low Bjorken-x which are not accessible at current accelerators. Moreover, these interactions can be described using pQCD and, in principle, the underlying theory is QCD rather than any phenomenological model. Additionally, it was previously shown [3, 5] that muon p_T distributions depend on the incident nuclei. Other composition measurements rely on the ratio of the measured electromagnetic energy to the number of muons [6, 7], the atmospheric depth X_{max}, where an air shower reaches the maximum number of particles [8], or multivariate analyses that combine several observables [9]. An analysis of laterally separated muons in IceCube complements these measurements of the cosmic ray mass composition.

2. Simulation of high p_T muon events

The fraction of laterally separated muons produced in air showers represents a rather small contribution to the total muon content inside the shower. Thus, simulating LS muon events with sufficiently large statistics using standard air shower simulation packages requires extremely high computational efforts. Moreover, previous studies have shown significant disagreement between simulations and data in the angular distribution of atmospheric muons [2, 4], especially for horizontal directions. This discrepancy is still not understood. Therefore, a detailed understanding of the underlying physics is crucial for the interpretation of such events requiring dedicated simulations.

The simulation of high p_T muon events is divided into two parts that are treated separately: the simulation of the central muon bundle and simulation of the isolated LS muon. These are re-combined after full shower propagation through the atmosphere. Although this violates energy conservation in the first interaction, the violation is below the 1% level and therefore negligible.

As a starting point cosmic ray air showers are simulated with primary energies in the relevant energy range using the CORSIKA package [10] with Sibyll 2.1 [11] to produce the typical central muon bundle signature as shown in Fig. 1. The primary spectrum is generated from a E^{-2} spectrum[1] in the range of 600 GeV $\leq E_{prim} <$ 100 EeV and re-weighted to the parametrization from Ref. [12] where the spectral index changes from -2.6 to -3.0 at $E_{knee} = 4$ PeV (the *"knee"*). A full shower simulation is performed assuming proton and iron primaries respectively using CORSIKA. The propagation of the particles through the ice and the photon emission are simulated using standard IceCube software.

Laterally separated muons produced in the air shower are simulated separately using the CRMC package [13] as an interface to get access to several hadronic interaction models. The production probabilities, as well as transverse momentum and energy distributions of high p_T particles produced in the first interaction can thereby be obtained from any hadronic interaction model. The production of particles with high transverse momentum from secondary interactions is highly suppressed due to significantly lower center-of-mass energies and is therefore neglected. All high p_T hadron energies and transverse momenta are drawn from these distributions for each individual primary that was used for the pre-simulated CORSIKA shower. Hence, the kinematic variables need only be generated in the limited phase space which is relevant to produce laterally separated muons that can reach the IceCube detector.

[1] Showers with primary energies below 1 PeV are generated from an $E^{-2.6}$ spectrum.

All types of secondary high p_T hadrons produced in the first interaction that predominantly contribute to the muon flux are taken into account:

- **pions and kaons:** $\pi^{\pm}$, $K^{\pm}$, K^0_L, $\bar{K}^0_L$.
- **prompt hadrons:** D^+, D^0, D^+_s, Λ^+_c, Ω^0_c, Ξ^+_c, Ξ^0_c, B^+, B^0, B^0_s, B^+_c, Λ^0_b, J/ψ, and anti-particles.
- **short-lived unflavored mesons:** η, η', ρ^0, ω, ϕ, and anti-particles.

Secondary contributions from high p_T kaons and unflavored mesons that decay into pions (K^0_L, K^0_S, η, η', ρ^0, $\rho^{\pm}$, ω, ϕ, and anti-particles), as well as from ϕ-mesons that can decay into kaons are also explicitly taken into account[2]. Since nitrogen is the most abundant element in the atmosphere (78.4%) it is used as target particle for all simulations. The contribution from oxygen (21.1%) has a similar mass number which obviates a distinctive treatment.

Figure 2 (left) shows the average number of high p_T hadrons produced per collision, the *"high p_T hadron abundance"*, for different primary energies obtained from EPOS-LHC [15] and QGSJet II-4 [16] assuming proton primaries. Since HIJING 1.3 [17] is the only available interaction model including a full modeling of the prompt component all distributions of prompt hadrons in this work are based on HIJING predictions[3] even if not explicitly denoted. Each LS muon event is weighted with the hadron abundance according to the spline interpolations shown in Fig. 2 (left, lines). Events with a high p_T hadron abundance below 10^{-4} are not taken into account because high p_T particle production is highly suppressed. Additionally LS muon detection from primaries with energies ~ 1 TeV is suppressed due to the natural shielding of the ice and by a subsequent high energy filtering (see Sec. 3).

Figure 2 (right) shows the transverse momentum distributions of various components for a primary energy of 1 PeV obtained from different hadronic models. A transition from soft to hard interactions that can be described in the context of pQCD is expected to be visible in these distributions as an exponential fall-off with a transition to a power law at $p_0 \simeq 2$ GeV [2]. Thus, the p_T

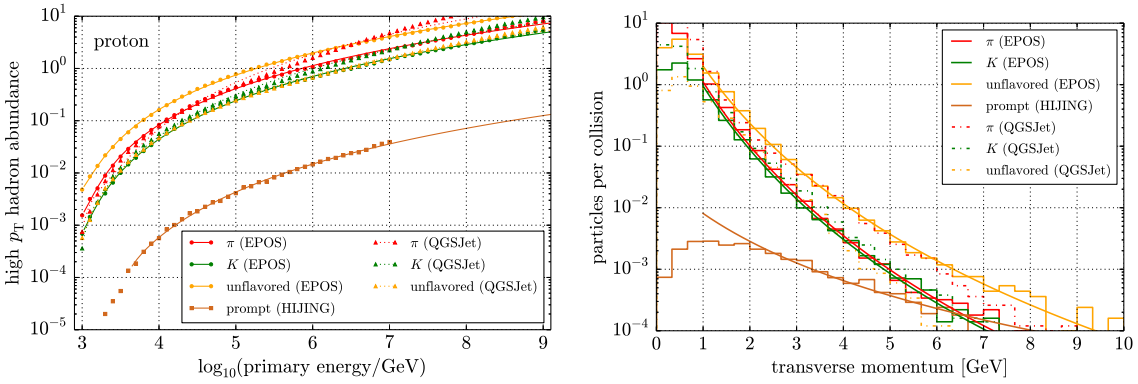

Figure 2: Left: High p_T hadron abundance for different interaction models. Right: Transverse momentum distribution of various hadrons with $E_h \geq 460$ GeV for a primary energy of 1 PeV as well as corresponding fits (lines) using Eq. (2.1).

[2]In the QGSJet model contributions from short-lived resonances are already included in the final state spectra of stable hadrons [14] therefore secondary decays into pions and kaons are not treated explicitly.

[3]HIJING pion, kaon, and unflavored distributions have rather good agreement with QGSJet predictions [5].

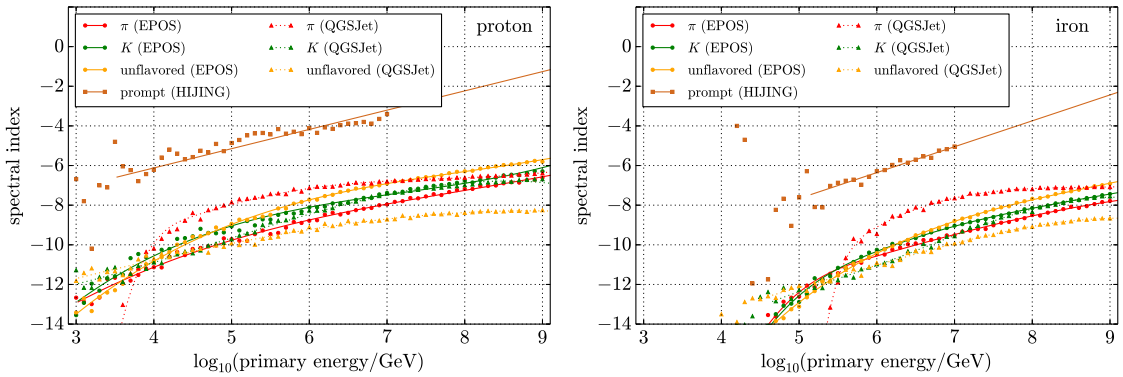

Figure 3: Spectral indices β obtained from fits using Eq. (2.1) applied to transverse momentum distributions for proton (left) and iron (right) primaries respectively and different hadronic models. The corresponding spline fits as a function of the primary energy are shown as lines.

distributions are fit with the QCD inspired *"modified Hagedorn function"* [18, 19]

$$\frac{dN}{dp_T} = \alpha \left(1 + \frac{p_T}{p_0}\right)^{\beta} \tag{2.1}$$

for $p_T \geq p_0 = 2$ GeV where α and β are allowed to vary. This function behaves exponentially at small p_T and as a pure power law at high p_T. The lines shown in Fig. 2 (right) represent these fits. Spectral indices $\beta(E_{\text{prim}})$ obtained for various initial energies are shown in Fig. 3 for proton (left) and iron primaries (right). The solid lines are spline interpolations used to define the spectral index as a function of the primary energy, where the end of the lines indicate where the hadron abundance drops below 10^{-4}. As expected, the p_T distributions flatten with increasing initial energy and the prompt component shows a generally harder spectrum.

Using these interpolations, the spectral index $\beta(E_{\text{prim}})$ is obtained according to the underlying primary energy for each pre-simulated CORSIKA event. The transverse momentum of the additional high p_T hadron is then generated from Eq. (2.1) over the range 1 GeV $\leq p_T \leq$ 12 GeV with a spectral index of $\beta = -1$, and re-weighted to the corresponding spectral index $\beta(E_{\text{prim}})$. This is done to increase the statistics of events carrying high p_T that predominantly produce large lateral separations. The energy distributions of hadrons are obtained analogously from different hadronic interaction models and several initial energies. The high p_T hadron energy of each event is then generated in the range $E_h \geq E_{\mu,\text{min}} = 460$ GeV from the distribution with the simulated energy closest to the underlying primary energy.

Propagation and decay of particles is performed using the Monte Carlo method from Ref. [12] to decide if a hadron decays or re-interacts with an air molecule within the atmosphere. The cross-sections of hadron-air[4] interactions are obtained from the underlying hadronic model. The decay probabilities as well as all relevant branching ratios of the different hadrons into muons are included in simulation via event weighting. To estimate energy losses due to the decay, the energy fractions

[4]The cross-sections of prompt hadrons which cannot be used as an initial particle in any interaction model are approximated by the corresponding kaon cross-section. Since the prompt cross-sections should be somewhat smaller this results in a small underestimation of the prompt flux.

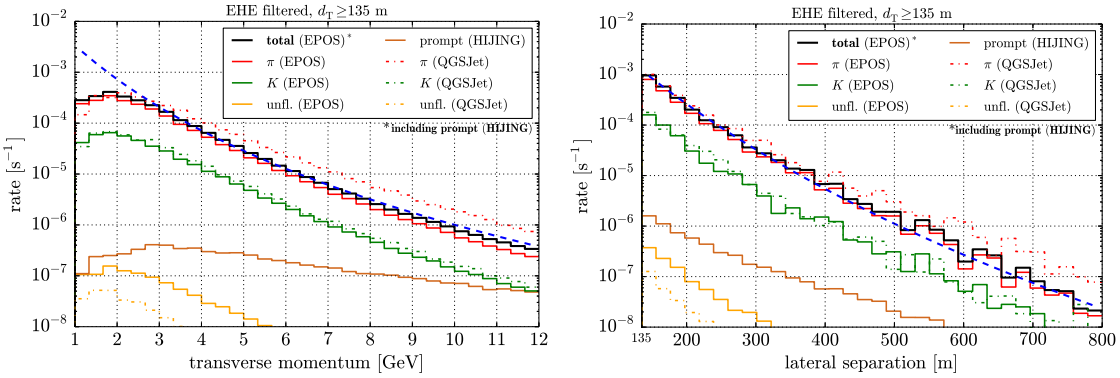

Figure 4: Transverse momentum (left) and lateral separation distribution (right) of simulated LS muon events in IceCube after EHE filtering and with separations above 135 m assuming proton primaries using different hadronic models. Also shown are fits using Eq. (2.1) applied to both distributions (blue lines).

E_μ/E_h of the resulting muons are obtained from PYTHIA 8.1 [20] simulations. Deflections caused by the Earth's magnetic field as well as multiple scattering in the atmosphere are negligible for the energies and lateral separations considered here [2]. Using standard IceCube software the propagation of the LS muon and the emitted photons in the ice is simulated. Finally, the LS muon and the pre-simulated muon bundle signals are combined and the detector response simulated to form a complete laterally separated muon event in IceCube.

3. Simulated LS muon distributions in IceCube

LS muons are selected from the IceCube high energy filter stream (*"EHE filter"*) which keeps events with at least 10^3 photoelectrons in the detector [2]. Additionally, only events with lateral separations larger than 135 m are considered as LS muon events. Figure 4 (left) shows the transverse momentum distribution of simulated LS muon events passing these selection criteria for proton primaries and various parent particles based on EPOS-LHC and QGSJet II-4. As expected, the contribution of events with $p_T \lesssim 2$ GeV is suppressed due to the constraint on minimum lateral separation despite the lower transverse momenta being overestimated (see Fig. 2). A fit using Eq. (2.1) applied to the total LS muon distribution based on EPOS for $p_T \geq p_0 = 3$ GeV (blue line) has a spectral index of $\beta = -6.89 \pm 0.06$. The same fit with the replacements $p_T \to d_T$ and $p_0 \to d_0 = 400$ m [2] applied to the lateral separation distribution shown in Fig. 4 (right) has a spectral index $\beta = -13.45 \pm 0.14$. A pure-iron composition assumption (not shown) results in steeper spectra with $\beta = -9.87 \pm 0.04$ for the transverse momentum and -15.50 ± 0.21 for the lateral distribution respectively. The prompt component shows a harder spectrum for both distributions. The simulations, including detector response, produce results consistent with those previously observed [2] and in accordance with pQCD predictions. Figure 5 (left) shows the spectral indices obtained from fits using Eq. (2.1) applied to p_T distributions within different simulated primary energy (top) and total charge intervals (bottom) for proton and iron primaries respectively. The simulated deposited total charge in the detector is given in units of the number of photoelectrons (NPE) which depends on the detector setup. It is approximately proportional to the energy loss in the detector and therefore closely related to the initial primary energy. Nearly

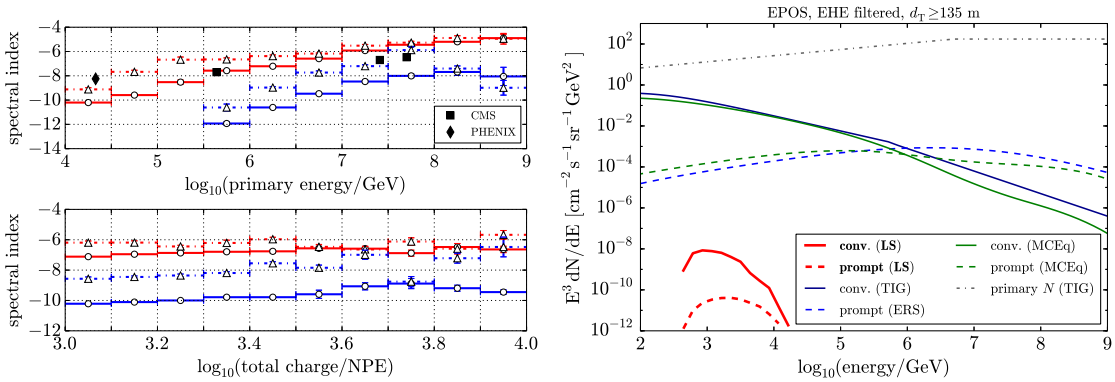

Figure 5: Left: Spectral indices of simulated p_T distributions within different primary energy (top) and total charge intervals in units of NPE (bottom) in IceCube. These are shown for proton (red) and iron primary interactions (blue) based on EPOS (circles) and QGSJet (triangles). Experimental data for proton-proton collisions from PHENIX [21] and CMS [22, 23] is shown for comparison. Right: Flux of LS muons in IceCube for proton primaries based on EPOS as well as muon flux predictions on surface from Ref. [12] (TIG), [24] (ERS), and [25] (MCEq) for comparison.

all LS muon events (96.1% for proton and 99.9% for iron primaries) are generated in the range 10 TeV $\leq E_{\text{prim}} \leq$ 1 EeV. The spectral indices show a clear separation between proton and iron assumptions. Also shown are spectral indices obtained from pion p_T distributions in proton-proton collisions from PHENIX at $\sqrt{s} = 200$ GeV [21] and of charged hadron distributions from CMS at $\sqrt{s} = 0.9$ TeV, 2.3 TeV, 7 TeV [22, 23]. The corresponding primary energies are given in the laboratory frame by $E_{\text{prim}} = (s - 2m_p^2)/2m_p$ with proton mass m_p and the underlying assumption that all but one nucleon of each colliding ion can be regarded as spectators only. Figure 5 (right) shows the simulated energy spectrum (scaled with E^3) of laterally separated muons assuming a pure-proton primary composition with EPOS in comparison to several theoretical predictions of the total muon flux on the surface [12, 24, 25]. Also shown is the primary spectrum used in this work [12]. The LS muon energy distribution peaks at $E_\mu \sim 1$ TeV since extremely high energy muons with large separations are highly suppressed due to the $1/E_\mu$ dependence in Eq. (1.1). The resulting total LS muon flux from proton primaries corresponds to an expected event rate of approximately 79,000 events in one year of IceCube high energy data. The event rate assuming pure-iron primary composition is roughly 21,000 events in one year of data. The corresponding event rates based on QGSJet simulations are approximately 25% higher (5% lower) for proton (iron) primaries.

4. Conclusion and outlook

Muons with high transverse momentum have been observed as double track signatures in IceCube [2]. The lateral separation of these muons can be used to study their kinematic distributions and their parent particle's hadronic interactions. A method to simulate laterally separated muons was presented, including an explicit treatment of different air shower components. The simulated p_T and lateral distributions as well as the energy spectrum after high energy filtering were shown. The expected LS muon event rate is between 21,000 and 79,000 events in one year of IceCube data depending on the primary mass composition.

An analysis of laterally separated muons in IceCube based on these simulations is in preparation. Several selection criteria as well as dedicated double track reconstructions [2] will be used to get a pure sample of LS muon events to draw conclusions on the underlying physics. The simulations enable, for example, studies on the treatment of hadrons producing muons and their p_T modeling for different hadronic interaction models. Upcoming versions of hadronic interaction models with a prompt contribution to the muon flux, for example Sibyll with charm [26], can be included to further improve the simulation of laterally separated muons. Moreover, it was shown that the distributions of LS muons depend on the incident nuclei and they can therefore be used to study the cosmic ray mass composition. This complements other composition measurements and enables studies on high energy interactions of intermediate nuclei at low Bjorken-x.

References

[1] A. Achterberg *et al.* (IceCube Collaboration), Astropart.Phys. **26** (2006) 155.

[2] R. Abbasi *et al.* (IceCube Collaboration), Phys. Rev. D **87** (2013) 012005.

[3] S. R. Klein, D. Chirkin for the IceCube Collab., in *Proc. of the 30th ICRC* (2007) [arXiv:0711.0353].

[4] M. G. Aartsen *et al.* (IceCube Collaboration), (2015) [arXiv:1506.07981].

[5] D. Soldin for the IceCube Collab., in *Proc. of the 18th ISVHECRI* (2014) [arXiv:1411.4448].

[6] M. G. Aartsen *et al.* (IceCube Collaboration), PoS(ICRC2015)338 these proceedings (2015).

[7] M. G. Aartsen *et al.* (IceCube Collaboration), PoS(ICRC2015)267 these proceedings (2015).

[8] D. Kang *et al.*, in *Proc. of the 16th ISVHECRI* (2010) [arXiv:1009.4902].

[9] M. G. Aartsen *et al.* (IceCube Collaboration), PoS(ICRC2015)334 these proceedings (2015).

[10] D. Heck *et al.*, Tech. Rep. FZKA 6019 (Forschungszentrum Karlsruhe GmbH, Karlsruhe, 1998).

[11] E. Ahn, R. Engel, T. Gaisser, P. Lipari, T Stanev, Phys. Rev. D **80** (2009) 094003.

[12] M. Thunman, G. Ingelman, P. Gondolo, Astropart. Phys. **5** (1996) 309.

[13] C. Baus, T. Pierog, R. Ulrich, http://web.ikp.kit.edu/rulrich/crmc.html (2014).

[14] S. Ostapchenko, EPJ Web Conf. **52** (2013) 02001.

[15] T. Pierog *et al.*, (2013) [arXiv:1306.0121].

[16] S. Ostapchenko, Phys. Rev. D **83** (2011) 014018.

[17] M. Gyulassy and X.-N. Wang, Comput. Phys. Commun. **83** (1994) 307.

[18] R. Hagedorn, Rev. del Nuovo Cim. **6N 10** (1984) 1.

[19] J. Adams *et al.* (STAR Collaboration), Phys. Rev. C **70** (2004) 044901.

[20] T. Sjöstrand, S. Mrenna, P. Skands, Comput. Phys. Commun. **178** (2008) 852-867.

[21] A. Adare *et al.* (PHENIX Collaboration), Phys. Rev. C **81** (2010) 034911.

[22] V. Khachatryan *et al.* (CMS Collaboration), JHEP **02** (2010) 041.

[23] V. Khachatryan *et al.* (CMS Collaboration), Phys. Rev. Lett. **105** (2010) 022002.

[24] R. Enberg, M. H. Reno and I. Sarcevic, Phys. Rev. D **78** (2008) 043005.

[25] A. Fedynitch *et al.*, in *Proc. of the 18th ISVHECRI* (2014) [arXiv:1503.00544].

[26] F. Riehn *et al.*, in *Proc. of the 18th ISVHECRI* (2014) [arXiv:1502.06353].